Electron Bremsstrahlung Hard X-Ray Spectra, Electron Distributions and Energetics in the 2002 July 23 Solar Flare

Gordon D. Holman, Linhui Sui[1], and Richard A. Schwartz[2]

Laboratory for Astronomy and Solar Physics, Code 682, NASA/Goddard Space Flight Center, Greenbelt, MD 20771

holman@stars.gsfc.nasa.gov, lhsui@stars.gsfc.nasa.gov, richard.schwartz@gsfc.nasa.gov

and

A. Gordon Emslie

Department of Physics, The University of Alabama in Huntsville, Huntsville, AL 35899

emslieg@uah.edu

ABSTRACT

We present and analyze the first high-resolution hard X-ray spectra from a solar flare observed in both X-ray/γ-ray continuum and γ-ray lines. The 2002 July 23 flare was observed by the Ramaty High Energy Solar Spectroscopic Imager (RHESSI). The spatially integrated photon flux spectra are well fitted between 10 and 300 keV by the combination of an isothermal component and a double power law. The flare plasma temperature peaks at 40 MK around the time of peak hard X-ray emission and remains above 20 MK 37 min later. We derive the evolution of the nonthermal mean electron flux distribution by directly fitting the RHESSI X-ray spectra with the thin-target bremsstrahlung from a double power-law electron distribution with a low-energy cutoff. We also derive the evolution of the electron flux distribution on the assumption that the emission is thick-target bremsstrahlung. We find that the injected nonthermal electrons are well described throughout the flare by this double power-law distribution with a low-energy cutoff that is typically between 20–40 keV. Using our thick-target results, we compare the energy contained in the nonthermal electrons with the

---

[1]The Catholic University of America

[2]SSAI

energy content of the thermal flare plasma observed by RHESSI and GOES. We find that the minimum total energy deposited into the flare plasma by nonthermal electrons, 2.6×10^{31} erg, is on the order of and possibly less than the energy in the thermal plasma. However, these fits do not rule out the possibility that the energy in nonthermal electrons exceeds the energy in the thermal plasma.

Subject headings: Sun: flares, Sun: X-rays, gamma rays

1. Introduction

Since its launch on 2002 February 5, the Ramaty High Energy Solar Spectroscopic Imager (RHESSI) has been obtaining unprecedented images and spectra of solar flares in hard X-rays and γ-rays (see Lin et al. 2000 for a description of the RHESSI instrument and its capabilities). The hard X-ray/γ-ray continuum traces energetic electrons accelerated in flares, while γ-ray lines trace accelerated ions (e.g., Hudson & Ryan 1995). The first (and, currently, the only) γ-ray line flare observed by RHESSI occurred on 2002 July 23. This observation provides a rare opportunity to compare electron and ion acceleration in a single flare.

This *Letter* focuses on electrons in the July 23 flare. Spatially integrated photon flux spectra are derived from the RHESSI data in the 10–300 keV energy range. These spectra are fitted with computations of the bremsstrahlung flux from model electron distribution functions to deduce the temporal evolution of the flare electrons. Hard X-ray images and imaged spectra are obtained and analyzed in Krucker et al. (2003) and Emslie et al. (2003), respectively. The flare γ-ray bremsstrahlung above 300 keV is discussed in Share et al. (2003) and Smith et al. (2003). A comprehensive summary of the flare observations and their implications is presented in Lin et al. (2003).

We obtain the hard X-ray spectra and their time evolution in Section 2. In Section 3 we derive mean electron flux distributions (Brown, Emslie & Kontar 2003) from the RHESSI spectra. Our mean electron flux distributions, obtained through forward fitting, are compared with those obtained by Piana et al. (2003) through a regularized inversion procedure. In Section 4, we make the assumption that the emission is thick-target bremsstrahlung and obtain the evolution of the electron flux distribution. We then use these flux distributions to compute the total electron energy flux and its time evolution, and the total energy in accelerated electrons. These are compared to the evolution of the energy content of the thermal plasma observed by RHESSI and GOES. Our results are discussed in Section 5.

2. X-Ray Spectra

The time history of the flare emission in three energy bands is shown in Figure 1a. RHESSI uses two sets of aluminum attenuators, known as thin shutters and thick shutters, to avoid saturating the detectors during large flares. The July 23 flare was observed in two attenuator states. The instrument was primarily in the A3 state, with both sets of attenuators in place. Early in the flare, before 00:26:08 UT, and late in the flare, after 00:59:21 UT, the instrument was in the A1 state, with only the thin shutters in place. There were also four brief periods during which the instrument switched from A3 to A1 and back to A3. These transitions in attenuator state are apparent in the time history of the lowest energy band in Fig. 1a. The flux calibration is currently uncertain during the four brief transition periods. These time periods appear as gaps in subsequent results derived from the data.

Spectral fits were obtained using the Solar Software (SSW) spectral analysis routine (SPEX, see Schwartz 1996, Smith et al. 2002). Before fitting the data, we corrected the observed counts for pulse pileup and decimation (see Smith et al. 2002). Background counts were subtracted from the data by linearly interpolating between the background levels before and after the flare. Because the attenuators substantially diminish the photon flux that reaches the RHESSI detectors at low energies, spectra obtained in the A1 state were fitted down to 10 keV photon energies, while spectra obtained in the A3 state were fitted down to 15 keV. The spectra were fitted up to 300 keV unless a contribution from background counts was significant below this energy. At times earlier than 00:26:00 UT, for example, spectral fits could not be obtained above 60 keV. We estimate the systematic uncertainty in the fluxes in each energy bin, which dominates the random (Poisson) noise at high count rates, to be 2% in the A3 state and 5% in the A1 state. The absolute uncertainty in the RHESSI flux measurements is currently unknown. These estimates were obtained by requiring the reduced χ^2 for our spectral fits to be on the order of one.

We have used a forward fitting procedure, for which we assume the spectral form of the incident flux. We used an isothermal bremsstrahlung spectrum plus a double power law, giving us 6 free parameters: the temperature (T) and emission measure (EM) of the isothermal component, lower (γ_L) and upper (γ_U) spectral indices and the photon energy at which the spectral break occurs ($\mathcal{E}_B$), and the normalization for the double-power-law spectrum, taken to be the photon flux at 50 keV (F_{50}). This is folded through the instrument response to provide the expected count rates. The free parameters are varied until a minimum χ^2 fit to the count rates is obtained.

Late in the flare, only the isothermal component is evident. During the early rise of the flare (A1 state), we found that the spectra could be fitted with a double power law alone.

An equally good fit could be obtained with the combination of an isothermal component and a double power law above ∼18 keV. The results of this fit are shown in Fig. 1. Since this thermal component is not required by the data, the temperatures and emission measures derived from these fits are not as well established as those derived from fits for later time intervals when the thermal component is visually apparent in the spectra (as in Fig. 3). We expect to obtain a better determination of the thermal contribution to these spectra when RHESSI's response to the continuum radiation and iron line complex below 10 keV are better understood.

The time history of the temperature of the isothermal component is shown in Fig. 1b (plus signs). The temperature rapidly rises to "superhot" values (Lin et al. 1981) as high as 40 MK. This hot thermal emission is consistent with the spectrum of the "coronal" source observed in RHESSI images (Emslie et al. 2003). The plasma gradually cools after the end of the first peak in the flare emission, with some reheating in subsequent peaks. The plasma temperature derived from the RHESSI spectra remains above 20 MK for at least 37 min after reaching its peak value. Temperatures derived from GOES data are shown for comparison (solid curve). Throughout the flare the temperatures derived from the RHESSI data are typically around 10 MK higher than those derived from the GOES data. These higher temperatures are expected for a multithermal plasma, since GOES is sensitive to lower photon energies than RHESSI.

The emission measure of the isothermal component is plotted in Fig. 1c (plus signs). Although the peak temperature is similar to that obtained by Lin et al. (1981) for the 1980 June 27 flare, the peak emission measure is thirty times greater, consistent with the higher X-ray intensity of this flare. The GOES emission measure (solid curve, scaled by a factor of 0.25) always exceeds the RHESSI emission measure, as expected for the lower temperatures obtained from GOES.

The spectral indices γ_L and γ_U, defined by Flux $\propto \mathcal{E}^{-\gamma}$, have values between 2.5 and 3.5 throughout most of the flare (Fig. 1d). These spectral indices and their time evolution are consistent with the spectra obtained for the "footpoint" sources observed in RHESSI images (Emslie et al. 2003). Earlier in the flare, before the impulsive rise at 00:27:00 UT, the spectral indices are much greater, on the order of 5 and 6.5. While $\Delta\gamma$ is between 1 and 2 before the impulsive rise, it is subsequently 0.5 or less. When the nonthermal spectrum is observable after 00:40:00 UT, it is best fit with a single power law. The break energy, plotted in Fig. 1e, increases from values below 50 keV before the impulsive rise of the flare to values in the range 70–125 keV afterwards. The time history of the photon flux at 50 keV is plotted in Fig. 1f. This closely follows the 40–100 keV light curve, as expected.

3. Mean Electron Flux Distributions

The mean electron flux (electrons cm^{-2} s^{-1} keV^{-1}) is the spatially averaged value of the electron flux weighted by the plasma density (Brown et al. 2003). These distributions are independent of any assumptions regarding the evolution of electrons in the source and, therefore, are well suited for comparison with electron distributions computed from theoretical flare models. Deducing the mean electron flux from a photon spectrum is equivalent to deducing the electron flux under the assumption that the radiation is thin-target bremsstrahlung.

In this paper, we compute the mean electron flux distribution for time intervals during the rise and main peak of the flare with 20-s integration times. We do this by assuming that the functional form of the mean electron flux distribution is a double power law with a low-energy cutoff. We fit the observed count-rate spectra with the bremsstrahlung spectra computed from this distribution and an isothermal distribution, using the same SPEX forward fitting technique described above. The results of these 7-parameter fits are shown in Figure 2. The derived temperatures and emission measures are not shown here, since they are similar to the values in Fig. 1. For these and subsequent computations in Section 4, the bremsstrahlung cross section of Haug (1997) is used with the Elwert (1939) correction.

As expected for thin-target bremsstrahlung, the power-law indices for the mean electron flux distribution (Fig. 2b) are smaller than the photon spectral indices (Fig. 1d) by about 1. The break energies (E_B) for the electron distributions (Fig. 2c) are higher than those for the photon spectra (Fig. 1e) because bremsstrahlung photons are produced by electrons with higher energies than the photon energy. The spectrum only begins to flatten at energies immediately below the break in the electron distribution. The photon spectrum flattens to about $\mathcal{E}^{-1}$ below the low energy cutoff, E_c, shown in Fig. 2d. The values for E_c were determined by allowing the fitting routine to find the highest value consistent with a minimum χ^2 fit. The normalization in Fig. 2e is $\overline{n}V\overline{F}$, where V is the volume of the emitting region, $\overline{n}$ is the mean density of the thermal plasma in the emitting volume, and $\overline{F}$ is the mean electron flux distribution integrated from E_c to the highest electron energy in the distribution (we used a value of 5 MeV).

The spectral fit in the 15–300 keV energy range for the time interval 00:30:00–00:30:20 UT is shown in the top panel of Figure 3. Plotted in the bottom panel are the residuals from this fit, defined as $(F_{obs}(\mathcal{E}) - F_{fit}(\mathcal{E}))/\sigma(\mathcal{E})$, where $\mathcal{E}$ is the photon energy, F_{obs} is the observed photon flux, F_{fit} is the photon flux given by the model at energy $\mathcal{E}$, and σ is the uncertainty in the observed flux. The uncertainty σ includes both the systematic uncertainty, discussed in Section 2, and the Poisson statistics, added in quadrature. The residuals are limited to about the $\pm 2\sigma$ level, but they are not random over the full energy range. The systematic deviation below 20 keV may be due to our currently uncertain knowledge of the steep RHESSI response function at low energies when both attenuators are in place, or to the contribution of lower temperature plasma to the thermal bremsstrahlung. An inaccurate background subtraction could explain any systematic trend above 200 keV. Of particular physical interest is the apparent systematic oscillation between 20 keV and 50 keV. This may indicate that our correction for pulse pileup is not entirely accurate. On the other hand, this oscillation might be real and be associated with X-ray photons Compton scattered in the photosphere (albedo) or partial ionization in the interaction region. These possibilities are considered by Alexander & Brown (2002) and Kontar et al. (2003), respectively.

Piana et al. (2003) derive mean electron flux distributions from this flare data using a direct inversion technique. Their results are quite different from the double power-law distributions obtained here, showing considerably more structure in the electron distributions. Both distributions provide an acceptable χ^2 fit to the photon spectra. The differences in these derived electron distributions highlight the fact that there is no unique electron distribution associated with an observed count-rate spectrum. Nevertheless, the spectral fits can rule out many models, and RHESSI's combination of high spectral and spatial resolution allows us to test physical processses and models that could not be adequately addressed with previous observations.

4. Thick-Target Flux Distributions and Energetics

Electron flux distributions (electrons s^{-1} keV^{-1}) are derived on the assumption that the nonthermal hard X-ray emission is thick-target bremsstrahlung (Brown 1971) and that the electron distribution is a double power law with a low-energy cutoff. The thick-target bremsstrahlung from this electron distribution is numerically computed and added to an isothermal bremsstrahlung component. The resulting photon spectra, determined by 7 free parameters, are fitted to the RHESSI count-rate spectra. The results are shown in Figure 4.

The upper electron power-law indices (triangles, Fig. 4b) are larger by about one than the upper photon spectral indices, as expected ($\delta_U \simeq \gamma_U + 1$). The lower power-law indices are only slightly steeper than the lower photon indices, however, because fewer electrons are present above the break energy than would have been present for a single power law. The upper power-law index of about 4.0–4.5, found throughout much of the flare, is consistent with the value estimated from radio spectral observations (White et al. 2003). The break energy (Fig. 4c) increases with time from values around 30 keV to values in excess of 200 keV.

The low-energy cutoff (Fig. 4d), as for the mean electron flux distribution (Section 3), was allowed to take the highest value consistent with a minimum χ^2 fit. This minimized the energy in nonthermal electrons and also provided the lowest values of χ^2. Except for a brief period between 00:40:40 UT and 00:42:00 UT, when the nonthermal part of the spectra was best fit with a single power law and a low-energy cutoff as high as 73 keV, this places the value of the low-energy cutoff near the photon energy at which the isothermal (exponential) photon spectrum flattens to the nonthermal power-law spectrum. We note that this location for the low-energy cutoff is comparable to that obtained with a hybrid thermal/nonthermal electron acceleration model in which the hot flare plasma and a tail of runaway electrons are produced simultaneously (Holman & Benka 1992, Benka & Holman 1994). The low-energy cutoff increases from around 20 keV before 00:26:00 UT to 30–40 keV after this time.

The distributions before 00:26:00 UT are also consistent with a double power law alone (no isothermal component) and a single power law with a high energy cutoff that increases from 40 keV at early times to as high as 100 keV at later times. However, we found that these spectra could not be adequately fit with a single power law with a low-energy cutoff (no isothermal component) or with an isothermal distribution alone.

The total electron flux, integrated over all electron energies, is plotted in Fig. 4e. It reaches its maximum value of 5×10^{36} electrons s^{-1} at 00:25:20 UT. Note that this is before the impulsive rise after 00:27:00 UT and the appearance of the much harder X-ray spectra and the γ-ray line emission.

We can compute the total density of nonthermal electrons by dividing the flux distribution function by the electron speed and the area of the thick-target interaction region and integrating over all electron energies. For an area of 10^{19} cm^2, on the order of that shown by the RHESSI image at 00:23:45 UT (see Krucker et al. 2003), this gives a density in suprathermal electrons of 6×10^7 cm^{-3} at 00:25:20 UT. Later in the flare the observed nonthermal source area is as low as 10^{17} cm^2, giving densities that are up to an order of magnitude higher. White et al. (2003), in interpreting their radio observations of the flare, deduce a nonthermal electron density of 10^{11} cm^{-3} above 10 keV at 00:35:00 UT. We obtain a density of 3×10^9 cm^{-3} at this time if the electron distrubution extends down to 10 keV. Most of the difference in these densities can be attributed to the flattening of the electron distribution below the break energy of 134 keV in our fit. If we were to extrapolate the part of the electron distribution that is relevant to the optically-thin radio observations, that above the break energy, down to 10 keV, the inferred density would be 2.4×10^{10} cm^{-3}.

The energy flux (solid curve with plus signs) and the total accumulated energy deposited into the flare plasma (dotted curve) by electrons with energies above E_c are plotted as a function of time in Fig. 4f. The energy flux (power) is obtained by multiplying the electron flux distribution derived for each 20-s interval times the electron energy and integrating over all energies above E_c. The accumulated energy is obtained by multiplying the energy flux at each time by the time interval (20 s) and obtaining the sum of these energies up to the time of interest. Note that about two-thirds of this energy is deposited before 00:26:00 UT. The total energy injected by these electrons during the whole flare is found to be 2.6×10^{31} erg.

The energies contained in the thermal plasmas observed by RHESSI (dot-dash line) and by GOES (solid line) are also plotted in Fig. 4f. Using the temperatures and emission measures derived from the observations, we are able to compute the product of the plasma density and energy, $n(3nkTV)$. We can also estimate the volume (V) of the thermal plasma observed by RHESSI from the RHESSI images (Krucker et al. 2003) and, using the emission measure (EM), derive the density $n = \sqrt{EM/V}$. Before 00:27:00 UT we estimate the volume to be 2×10^{28} cm^3, and after 00:27:00 UT, during the main phase of the flare, we obtain 4×10^{27} cm^3. For an emission measure of 5×10^{49} cm^{-3} (Fig. 1c), for example, typical of the main phase of the flare, we obtain a density of 1×10^{11} cm^{-3} for the hot plasma observed by RHESSI. Writing the plasma energy as $3kT\sqrt{EM \cdot V}$, we us these volumes for both RHESSI and GOES to obtain the curves plotted in the figure. The discontinuity in the curves at 00:27:00 UT is an artifact of our step function approximation for the volume change around that time.

We see from Fig. 4f that, even with the low-energy cutoffs derived here, the accumulated energy in the nonthermal electrons is comparable to the energy in the thermal plasma observed by both RHESSI and GOES. The peak energy in the thermal plasmas, 6.6×10^{30} erg for RHESSI and 1.1×10^{31} erg for GOES, is reached at about 00:36:00 UT. The energy deposited by the nonthermal electrons may be somewhat less than the energy in the thermal plasma if the volume of the plasma observed by GOES is at least $\sim$4 times greater than assumed. Otherwise, the energy is equal to or exceeds the thermal energy.

Electron distributions with low-energy cutoffs lower than the values derived here are also consistent with the RHESSI spectra. Therefore, the energy deposited by the nonthermal electrons may be greater. Emslie (2003) shows that the temperature of the target plasma limits the energy that can be deposited into the plasma. The energy injected into the plasma is significantly less than the electron energy computed above a low-energy cutoff if the cutoff energy is less than $5kT$, where T is the temperature of the target plasma. Taking the temperature of the target plasma to be equal to or less than the temperatures we derived from the spectral fits, the low-energy cutoffs derived here all exceed $5kT$. Therefore, the computed injection energies are accurate unless undetected higher temperatures are present in the interaction region. Using our derived temperatures and the results of Emslie, we can compute the maximum energy these electrons could have injected into the flare plasma. We find this to be 4×10^{34} erg. It is unlikely that the electrons deposited this much energy into the flare plasma, since it is greater than the maximum total energy that has been deduced previously for even the largest solar flares.

5. Conclusions

The RHESSI spectra presented and analyzed here are the most detailed hard X-ray spectra ever obtained for a large flare. Although these spectra are well fitted by isothermal (exponential) and double power-law photon distributions, fitting these spectra with the bremsstrahlung spectra computed from model electron distributions is an important part of our analysis. The electron distributions allow a more physical interpretation of the data and smooth out the unphysically sharp break in the double power-law photon spectrum. Even fits with a double power-law electron distribution, however, show systematic residuals at the level of a few percent, as in Fig. 3b. Understanding these residuals will also be an important part of the future analysis of RHESSI spectra.

The July 23 flare hard X-ray spectral data provide support for the longstanding impression that the energy in accelerated electrons is a major part of the energy released in many, if not all, flares. Our result for the energy injected by nonthermal electrons depends, however, on our nonthermal, thick-target interpretation of the double power-law fits. One compelling alternative is that the X-ray emission observed in the early rise phase of the flare (before 00:26:00 UT) is, at least in part, thin-target bresstrahlung from the corona (Lin et al. 2003). The extended size of the X-ray source at this time is suggestive of this interpretation. Another possibility is that the emission is from a multithermal plasma, but high temperatures would be required for this interpretation. A study of these alternatives requires additional modeling beyond the scope of this paper.

The information extracted from these spatially integrated spectra can only be fully appreciated and understood through comparison with RHESSI images and imaged spectra, and with related observations of the flare. A synthesis of the overall flare data and a discussion of possible interpretations are contained in Lin et al. (2003).

This work was supported in part by the RHESSI Project and the NASA Sun-Earth Connection program. We thank Sally House for translating the bremsstrahlung codes from Fortran into IDL, Paul Bilodeau for his help with the SPEX software and with integrating the bremsstrahlung codes with the SPEX software, and Kim Tolbert for her help with the RHESSI data analysis software. We thank Brian Dennis for his many comments on the manuscript. We also thank Hugh Hudson, Nichole Vilmer, and Stephen White for their helpful comments. This work would not have been possible without the dedicated efforts of the entire RHESSI team.

REFERENCES

Alexander, R. C. & Brown, J. C. 2002, Sol. Phys., 210, 407

Benka, S. G. & Holman, G. D. 1994, ApJ, 435, 469

Brown, J. C. 1971, Sol. Phys., 18, 489

Brown, J. C., Emslie, A. G. & Kontar, E. P. 2003, ApJ, this issue

Elwert, G. 1939, Ann. Physik, 34, 178

Emslie, A. G. 2003, ApJ, this issue

Emslie, A. G., Kontar, E. P., Krucker, S. & Lin, R. P. 2003, ApJ, this issue

Haug, E. 1997, A&A, 326, 417

Holman, G. D. & Benka, S. G. 1992, ApJ, 400, L79

Hudson, H. & Ryan, J. 1995, ARA&A, 33, 239

Kontar, E. P., Emslie, A. G., Krucker, S. & Lin, R. P. 2003, ApJ, this issue

Krucker, S., Hurford, G. J. & Lin, R. P. 2003, ApJ, this issue

Lin, R. P., Schwartz, R. A., Pelling, R. M. & Hurley, K. C. 1981, ApJ, 251, L109

Lin, R. P., & the HESSI Team. 2000, in ASP Conf. Ser. 206, High Energy Solar Physics – Anticipating HESSI, ed. Ramaty, R., & Mandzhavidze, N. (San Francisco: ASP), 1

Lin, R. P., et al. 2003, ApJ, this issue

Piana, M., Massone, A. M., Kontar, E. P., Emslie, A. G., Brown, J. C. & Schwartz, R. A. 2003, ApJ, this issue

Schwartz, R. A. 1996, "Compton Gamma Ray Observatory Phase 4 Guest Investigator Program: Solar Flare Hard X-ray Spectroscopy," Technical Report, NASA Goddard Space Flight Center

Share, G., Murphy, R. J., Lin, R. P., Smith, D. M. & Schwartz, R. A. 2003, ApJ, this issue

Smith, D., et al. 2002, Sol. Phys., 210, 33

Smith, D. M., Share, G. H., Murphy, R. J., Schwartz, R. A., Shih, A. Y., & Lin, R. P. 2003, ApJ, this issue

White, S. M., Krucker, S., Shibasaki, K., Yokoyama, T., Shimojo, M. & Kundu, M. R. 2003, ApJ, this issue

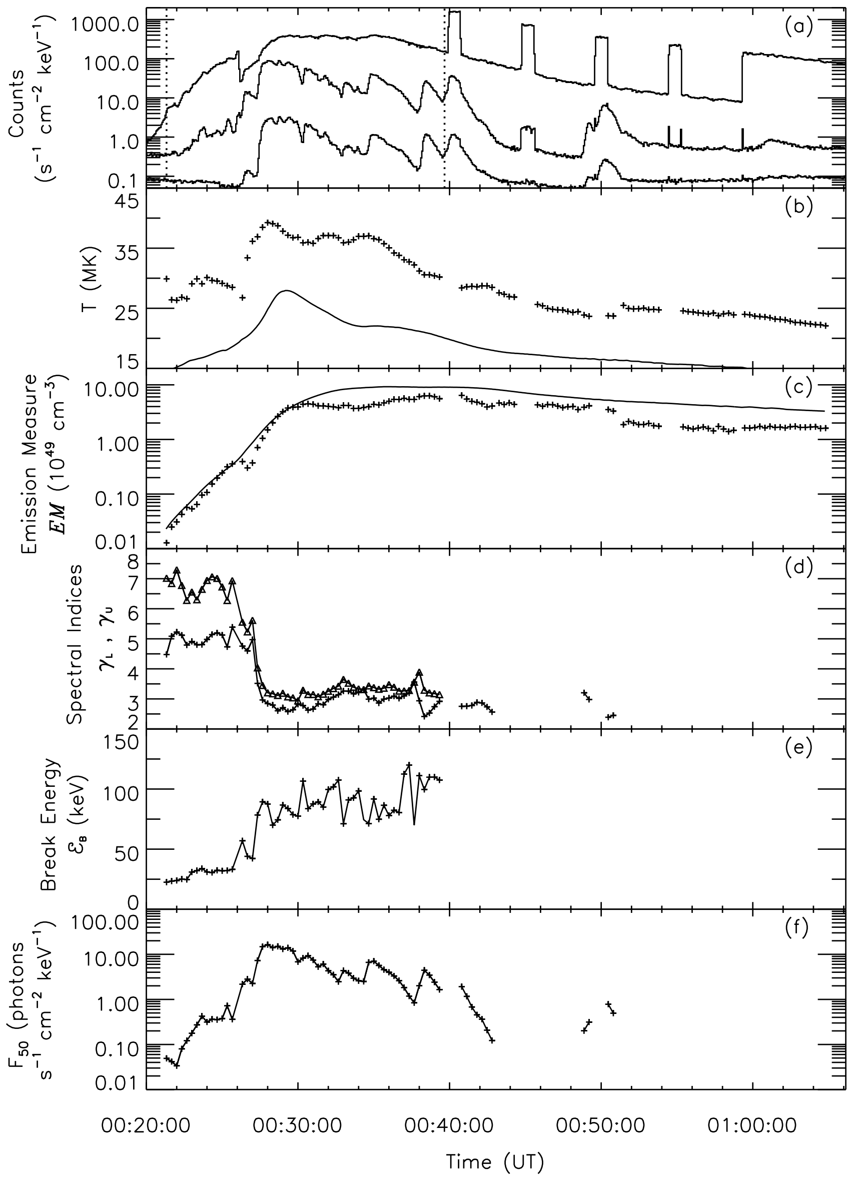

Fig. 1.— RHESSI X-ray light curves and time history of fit parameters. (a) Light curves in three energy bands, scaled to avoid overlap. The energy bands and scale factors are 12–40 keV (top curve, $\times 0.6$), 40–100 keV (middle curve, $\times 3$), and 100–300 keV (bottom curve, $\times 1$). The dotted vertical lines show the start time and the end time for the results of Fig. 2. (b) Time history of the temperature of the isothermal component (20-s time resolution, plus signs). The solid curve is the temperature derived from GOES data. (c) Time history of the isothermal emission measure (plus signs). The solid curve is the emission measure derived from GOES data, scaled by a factor of 0.25. (d) Time history of the double power-law spectral indices (spectral index below break, plus signs; spectral index above break, triangles). (e) Time history of the break energy in the double power-law spectra. (f) Time history of the photon flux at 50 keV, determined from the double power-law fit.

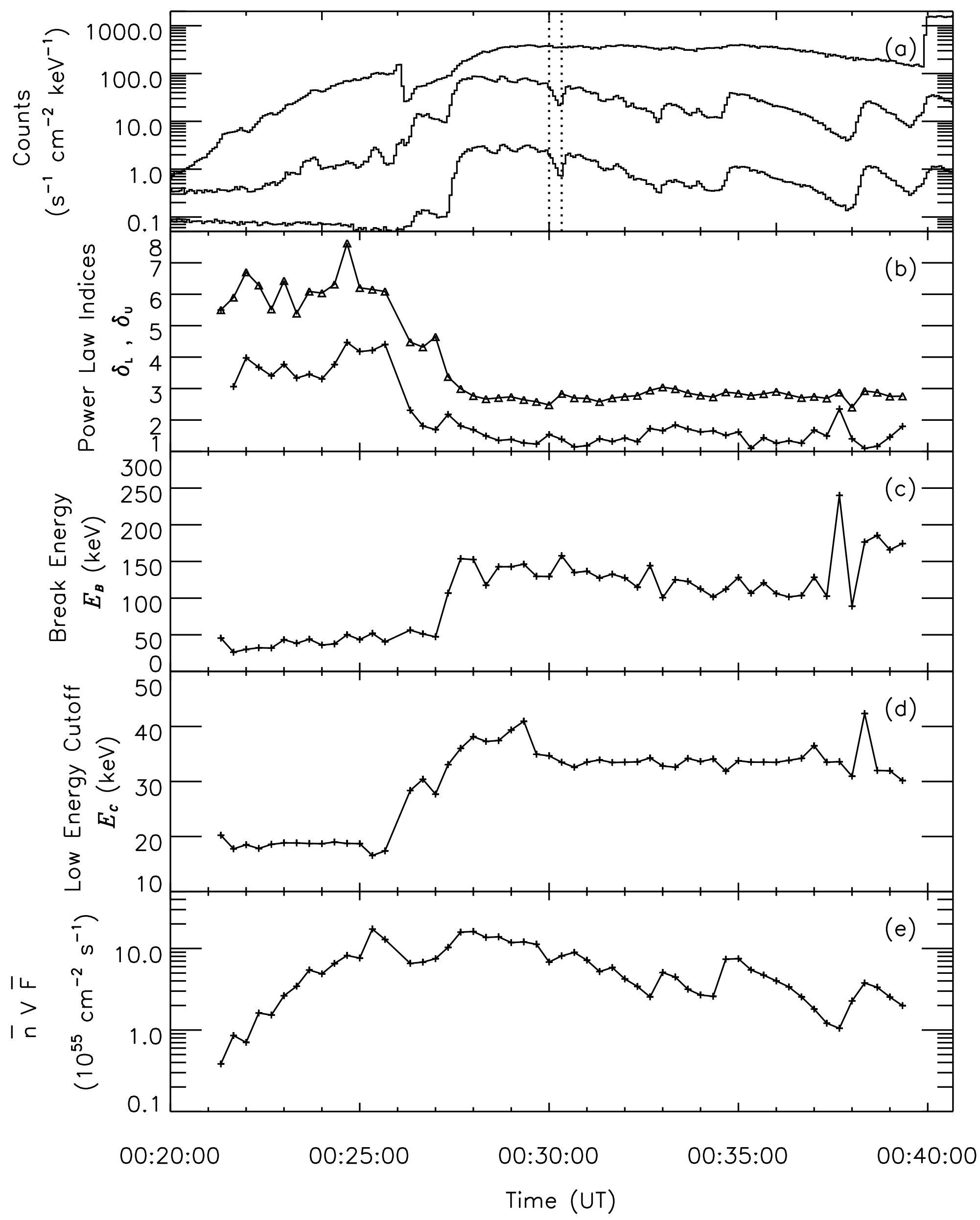

Fig. 2.— Time history of mean electron flux fit parameters. (a) Light curves in three energy bands (same bands and scale factors as Fig. 1a). The dotted vertical lines show the beginning and end of the integration time interval for the spectrum in Fig. 3. (b) Time history of the upper and lower power-law indices (20-s time resolution, same symbols as Fig. 1d). (c) Time history of the break energy in the double power-law mean electron flux distribution. (d) Time history of the low-energy cutoff in the mean electron flux distribution. (e) Normalization of the mean electron flux distribution (see text).

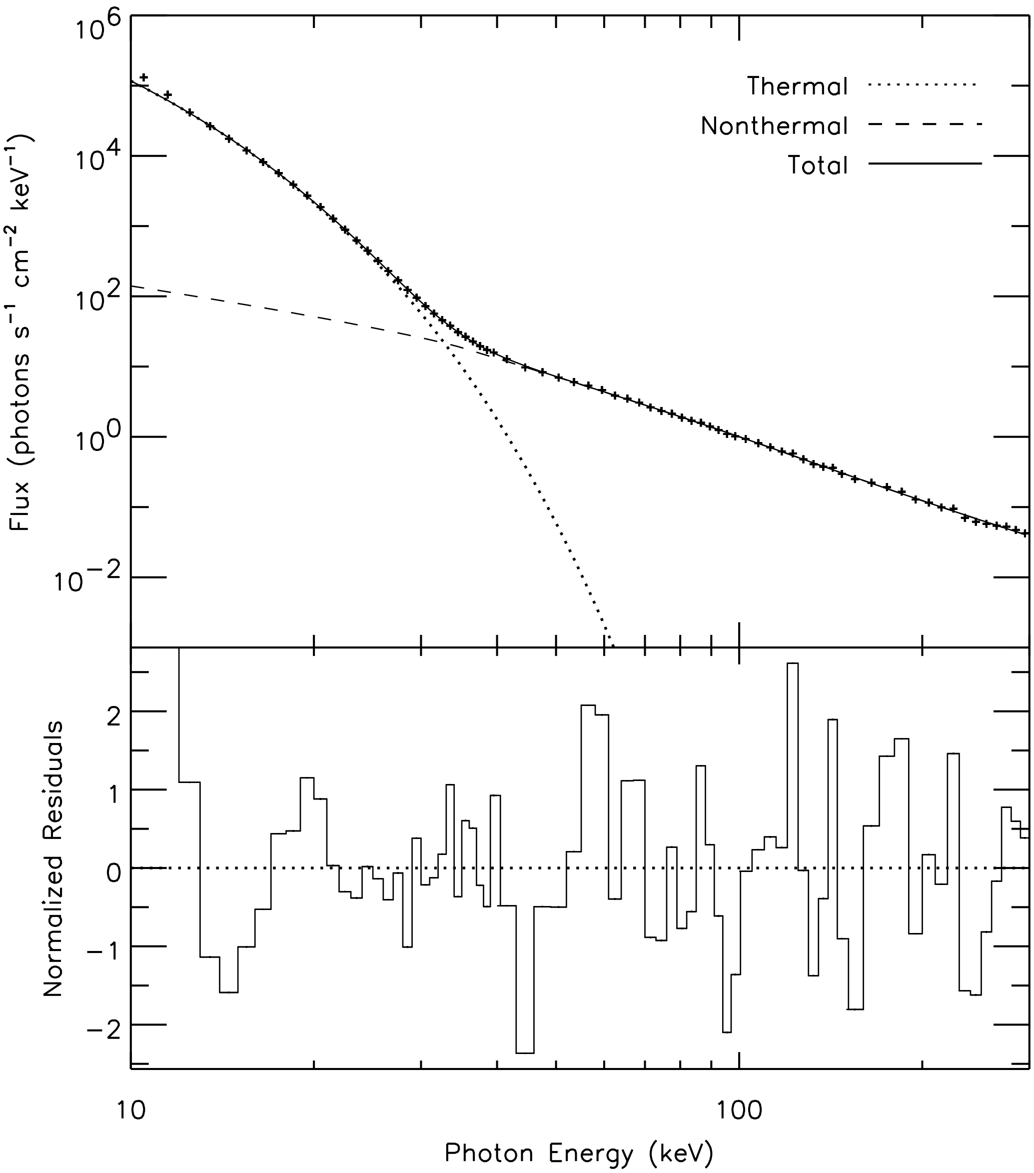

Fig. 3.— Fit and residuals for the 00:30:00–00:30:20 UT time interval. The fit in the upper panel is the bremsstrahlung from an isothermal plasma (dotted curve) and a double power-law mean electron flux distribution (dashed curve). The solid curve is the total fit. The best fit parameters were $EM = 4.1 \times 10^{49}$ cm^{-3}, $T = 37$ MK, $\overline{n}V\overline{F} = 6.9 \times 10^{55}$ cm^{-2} s^{-1}, $E_c = 34$ keV, $\delta_L = 1.5$, $E_B = 129$ keV, and $\delta_U = 2.5$ with a reduced χ^2 of 0.94. The data points are represented by plus signs. The residuals in the bottom panel are defined as the observed flux minus the model flux divided by the estimated one sigma uncertainty in each data point.

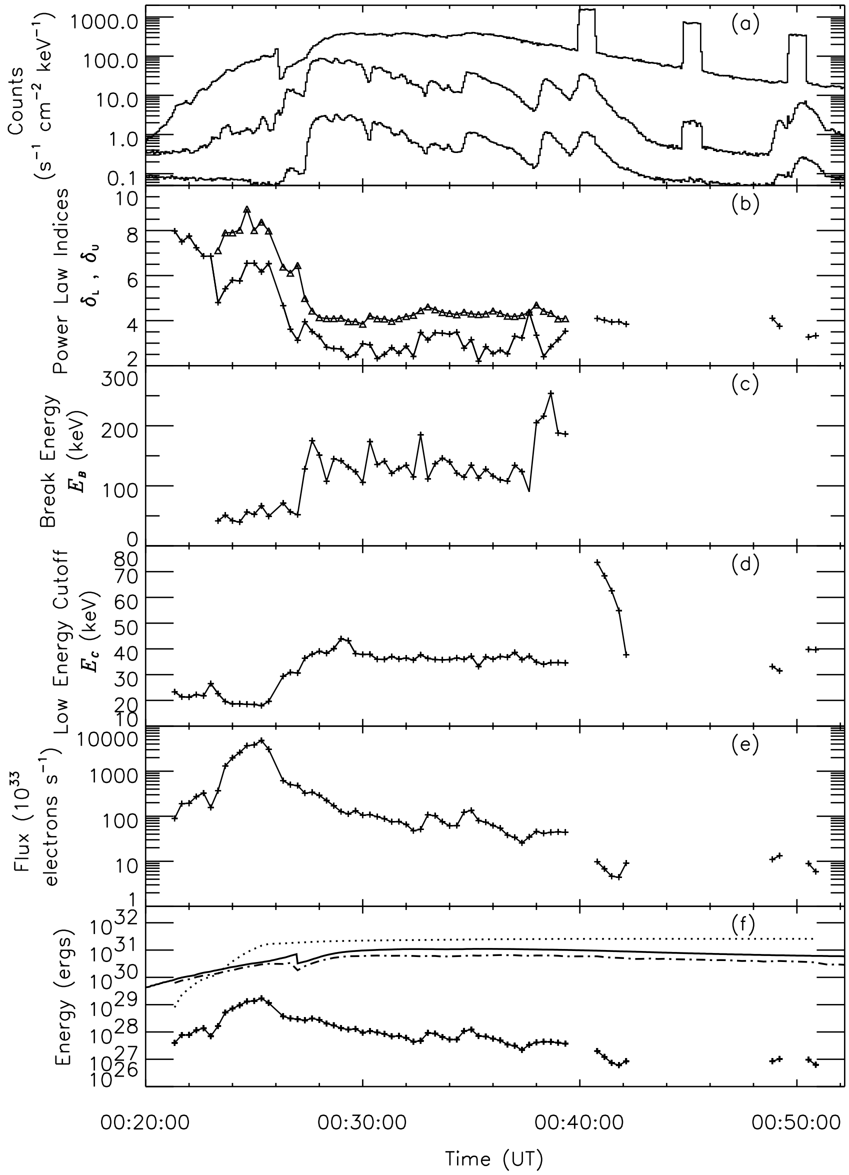

Fig. 4.— Thick-target bremsstrahlung electron flux distribution fit parameters and energetics. (a) X-ray light curves in three energy bands (see Fig. 1a). (b) Time history of the upper and lower power-law indices (20-s time resolution, same symbols as Fig. 1d). (c) Time history of the break energy in the double power-law electron flux distribution. (d) Time history of the low-energy cutoff in the electron flux distribution. (e) Time history of the integrated (over all electron energies) electron flux. (f) Thermal and nonthermal energetics. The time history of the energy in the GOES (solid line) and RHESSI (dot-dash line) isothermal fits is plotted using volumes estimated from RHESSI images (see text). This is compared to the accumulated energy in nonthermal electrons (dotted curve). The lower curve, marked with plus signs, is the energy injection rate (erg s^{-1}).